SSRG International Journal of Civil Engineering
ISSN: 2348-8352/ https://doi.org/10.14445/23488352/IJCE-V13I8P120

Volume 13 Issue 8, 324-341, August 2026

Original Article

Flexural Performance of Reinforced Concrete Beams Incorporating Cement-Bonded Fly Ash Aggregates as Partial Replacement of Natural Coarse Aggregate: Experimental Investigation, ANN Modelling, and Durability Assessment

Dakshayini R S[1], Urmila R. Kawade[2], Rudresh A N[3], Amey Raju Khedikar[4], Sandhya V[5], Kamaldeep[6], Prashant Sunagar[7]

[1]*Department of Civil Engineering, Malnad College of Engineering, Hassan, Karnataka, India.*
[2]*Department of Civil Engineering, Dr.V.V.Patil COE, Ahilyanagar, Maharashtra, India.*
[3]*Department of Civil Engineering, ATME College of Engineering, Mysuru, Karnataka, India.*
[4]*Department of Civil Engineering, Tulsiramji Gaikwad Patil College of Engineering and Technology, Nagpur, India.*
[5]*Department of Civil Engineering, Dayananda Sagar Academy of Technology and Management, Kanakapura Road, Bengaluru, India.*
[6]*School of Electrical Engineering, Shri Mata Vaishno Devi University, Jammu and Kashmir, India.*
[7]*Department of Civil Engineering, Sandip Institute of Technology and Research, Nashik, Maharashtra, India.*

[7]*Corresponding Author : prashant.sjce@gmail.com*

Received: 17 April 2026 Revised: 10 June 2026 Accepted: 19 August 2026 Published: 31 August 2026

Abstract - *The rising demand for natural coarse aggregate and its consequences have necessitated investigations into alternative aggregates from industrial sources. The structural performance and durability of reinforced concrete beams with cement-bonded Fly Ash Aggregate (FAA) at 25%, 50%, 75%, and 100% of the volume of natural coarse aggregate has been investigated. FAA was prepared by pelletisation of fly ash and cement at a 95:05, 90:10, and 85:15 mass ratio. The beams were of 100 mm × 150 mm cross-section and 1350 mm span, reinforced with 8 mm and 10 mm deformed bars and subjected to four-point bending test. The tests determined the Cracking Load (Pcr), Service Load (Psl), Ultimate Load (Pu), mid-span deflection, crack width, ductility index and energy absorption of FAA RC beams. The durability characteristics of FAA RC beams were also tested for Rapid Chloride Penetration (RCPT), water absorption, sorptivity and carbonation. The experimental results indicated that FAA3 (85:15) at 25% of natural aggregate replacement achieved a higher compressive strength (40.91 MPa) at 28 days than conventional M25 concrete (37.43 MPa). Furthermore, beams made with 25% FAA3 (85:15) sustained an ultimate load equal to that of the control beams for 8 mm tension reinforcement (42.11 kN in both cases) and 4.0% lower for 10 mm reinforcement (50.11 kN against 52.21 kN). At service load, the 8 mm FAA3 beams deflected 9.3% more than the corresponding control beam (4.48 mm against 4.10 mm), whereas the 10 mm FAA3 beams deflected 23.2% less (3.15 mm against 4.10 mm); the maximum crack width at service load was reduced by 9.9% in the 8 mm series and by 39.8% in the 10 mm series. The 25% FAA3 beams with 8 mm reinforcement also showed a 30.8% higher ductility index and 31.5% higher energy absorption than the control. The chloride penetration of all the mixes falls within the ASTM C1202 category for moderate chloride penetration of concrete. A feedforward artificial neural network of 5-6-4-1 topology, trained on the experimental data together with data drawn from the literature, predicted the ultimate load with R2 = 0.9921 and RMSE = 0.72 kN on an independent test set, outperforming a linear regression model (R2 = 0.934). The results indicated that 25% replacement level of natural aggregate with cold-bonded FAA3 (85:15) is a viable and eco-friendly alternative to natural aggregate in RC beams.*

Keywords - *Fly Ash Aggregate, Pelletisation, Cold-bonded aggregate, Reinforced concrete beam, Flexural behaviour, Crack width, Ductility, Artificial Neural Network, Durability, Chloride penetration.*

1. Introduction

The demand for natural aggregates to produce concrete is high, with around 40 billion tonnes of natural aggregate used in the concreting process every year in the world [1]. Around 4.5 billion tonnes of natural aggregate is consumed every year in the construction industry of India alone. Furthermore, the mining of sand and gravel from natural riverbeds are being restricted to preserve these ecosystems. Around 220 million tonnes of fly ash is produced by power plants that burn coal every year in India. Around 66% of the available fly ash is currently utilised [2]. The pelletisation of fly ash with cement into cold-bonded pellets that can act as artificial concrete aggregate presents a solution to these two problems.

The strength of cold-bonded fly ash aggregate (FAA) is developed through the chemical reaction of the fly ash with cement to produce pozzolanic compound and cementite after curing [3, 4]. The specific gravity of FAA is between 1.5 and 1.7, which is approximately 40 to 45% less than natural granite aggregates (2.65 to 2.75) [5, 6].

Hence, the use of FAA in concretes produces lightweight concretes that are advantageous in the construction of high-rise buildings that require fewer foundations and support columns [5, 6]. Kayali [7] has found that concretes made with pelletized fly ash aggregate exhibit high compressive strength of over 50 MPa when prepared with the appropriate ingredient proportions.

Although several investigations have been carried out on the compressive and splitting tensile strength of concretes containing cold-bonded fly ash aggregates [8-11], there is a lack of investigations on the flexural behaviour of reinforced concrete beams made using FAA. Swamy and Lambert [12] investigated the flexural behaviour of RC beams made with sintered fly ash aggregate. It was found that the strengths of these beams are comparable to those made with normal-weight aggregate concretes.

Arivalagan [13] investigated the flexural behaviour of beams where the cement was partially replaced with fly ash, but where the aggregate in the concretes remained natural. To the authors' knowledge, the present study is the first to combine, within a single programme, cold-bonded FAA manufactured at three different fly ash-to-cement ratios, reinforced concrete beams tested with two different tension bar diameters, a durability assessment of the resulting concrete, and an artificial neural network model for predicting the ultimate load of such beams from test data.

The main aim of this research is to investigate the flexural behaviour and durability characteristics of beams made with cold-bonded FAA of different ratios at different replacement levels of natural aggregate, and determine the best proportion and level of replacement of natural aggregate with cold-bonded FAA.

The results of this research will allow others to gain a better understanding of the mechanics of flexural members made with artificial aggregate concretes and will provide them with a tool to easily and accurately predict the performance of such beams.

2. Theoretical Background and Governing Equations

2.1. Cracking and Ultimate Moment Capacity (IS 456:2000 / ACI 318-19)

For a singly reinforced rectangular RC beam, the cracking moment M_cr is determined by the modulus of rupture of concrete and the section modulus of the gross (uncracked) cross-section:

$$M_{cr} = \frac{f_r I_g}{y_t} \quad (1)$$

where $f_r = 0.7\sqrt{f_{ck}}$(MPa) is the modulus of rupture according to IS 456:2000 [16]

The nominal ultimate flexural moment capacity of an under-reinforced section, based on limit state design principles in IS 456:2000, is expressed as

$$M_u = 0.87 f_y A_{st}(d - 0.42 x_u) \quad (2)$$

in which the neutral axis depth at the ultimate limit state is

$$x_u = \frac{0.87 f_y A_{st}}{0.36 f_{ck} b} \quad (3)$$

For beams subjected to symmetrical four-point loading, the applied maximum bending moment is

$$M = \frac{Pa}{2} = \frac{PL_{eff}}{6} \quad (4)$$

where P is the total applied load, $a = \frac{L_{eff}}{3}$ is the shear span, and L_{eff} is the effective span. The theoretical cracking and ultimate loads are therefore obtained by combining Eqs. (1)–(4), providing a rational benchmark for comparison with the experimental results.

2.2. Effective MI and Mid-Span Deflection

To account for stiffness degradation after cracking and before full section cracking, the effective MI, I_{eff}, is evaluated using the Branson-type formulation as

$$I_{eff} = I_{cr} + (I_g - I_{cr})\left(\frac{M_{cr}}{M_a}\right)^3 \leq I_g \quad (5)$$

The corresponding mid-span deflection under third-point loading is calculated from elastic beam theory as

$$\delta = \frac{P{L_{eff}}^3}{28 E_c I_{eff}} \quad (6)$$

where $E_c = 5000\sqrt{f_{ck}}$(MPa) is the modulus of elasticity of concrete as recommended by IS 456:2000. Equations (5) and (6) are used to estimate theoretical service-load deflections and to assess the degree of agreement between analytical predictions and measured beam responses.

Fig. 1 Experimental programme flowchart

2.3. Ductility Index

The deformation capacity of the beam beyond steel yielding is quantified through the displacement ductility index, defined as

$$\mu_{\Delta} = \frac{\delta_u}{\delta_y} \tag{7}$$

2.4. Crack Width Prediction

The surface crack width at the tensile face is estimated by incorporating the effects of bar spacing, cover, neutral axis depth, and mean steel strain. The crack width is expressed as

$$w_k = \frac{3a_{cr}\varepsilon_m}{1 + \frac{2(a_{cr} - c_{min})}{h - x}} \tag{8}$$

The mean strain, ε_m, accounting for tension stiffening, is given by

$$\varepsilon_m = \varepsilon_1 - \frac{b(h-x)(a-x)}{3E_sA_{st}(d-x)} \tag{9}$$

where $\varepsilon_1$is the steel strain at the considered section, $E_s$is the modulus of elasticity of steel, and ais the depth to the point where crack width is evaluated. The analytically predicted crack widths are compared with experimentally measured values obtained using optical microscopy.

2.5. Energy Absorption Capacity

The energy absorption capacity of each beam specimen using the trapezoidal integration rule:

$$E_{abs} = \sum \frac{(P_i + P_{i+1})}{2}(\delta_{i+1} - \delta_i) \tag{10}$$

where $P_i$and $P_{i+1}$are two successive load ordinates and $\delta_i$and $\delta_{i+1}$are the corresponding mid-span deflections. The resulting value of $E_{abs}$is reported in kN·mm and represents the overall toughness of the beam under flexural loading.

2.6. Sorptivity

The capillary absorption of concrete is characterized through sorptivity, which relates cumulative water absorption per unit area to the square root of elapsed time. The relationship is written as

$$I = S\,t^{\frac{1}{2}} + b \tag{11}$$

3. Materials and Experimental Programme

3.1. Experimental Programme

The programme was executed in four phases: procurement and characterisation of raw materials, manufacture of FAA and testing of the FA aggregate, preparation and casting of concrete specimens and testing of the solidified concretes, and testing of the durability properties of the concretes. A flowchart of the experimental programme is presented in Figure 1.

3.2. Raw Materials

3.2.1. Cement

OPC 53 grade cement from Birla Corporation Ltd was used with properties as per IS 12269:2013 and IS 4031:1988; SG = 3.14, standard consistency = 28%, initial setting time (IST) = 38 min, final setting time (FST) = 248 min, 28 day compressive strength (fck) = 31.8 MPa (3d), 42.6 MPa (7d), 54.2 MPa (28d), and loss on ignition (LOI) = 1.84%.

3.2.2. Fine Aggregate

FA local sand passing 4.75 mm & retained on 2.36 mm sieve falls under Zone III as per IS 383:2016 with FM=2.39, SG=2.681, WA=1.2% and BD=1641 kg/m³.

3.2.3. Natural Coarse Aggregate

CA (crushed granite) with the following properties, reported in full in Table 1: SG = 2.73, WA = 0.41%, BD = 1601.1 kg/m³, AIV = 27.11%, ACV = 25.11%, FM = 7.01.

3.2.4. Fly Ash

Class F FA (Raichur Thermal Power Station) to be used as the primary FAA with the following composition: SiO_2 = 60.4%, Al_2O_3 = 28.2%, Fe_2O_3 = 4.8%, CaO = 1.6%, SO_3 = 0.42%, LOI = 1.94%; SG = 2.01 and Blaine fineness = 3820 cm²/g as per IS 3812 (Part 1):2003

Fig. 2 Cement-bonded fly ash aggregate pellets collected from the pelletiser drum

3.2.5. Water and Superplasticiser

The water used in the preparation of both the FAA and the FC was the potable water that was used in the manufacturing of both the aggregate and the concrete. A naphthalene-based superplasticiser (Glenium 720 from BASF India) was incorporated into the FAA mix at a dosage of 1.0% of the total mass of the cement and fly ash in order to counteract the additional water demand introduced by the porous nature of the FAA.

3.3. Manufacture and Characterization of Fly Ash Aggregates

3.3.1. Pelletisation of Fly Ash Aggregates

FAA was prepared using a 50 L tilting drum mixer with FA: C ratios of 95:05 (FAA1), 90:10 (FAA2), and 85:15 (FAA3). The dry FAA powders were mixed for 2 min, and water was added to enable pelletization at 20 rpm (optimal moisture content) for 4-6 min. Pellets were air-dried for 24 h, followed by water curing for 7 days. Samples were sieved to separate coarse FAA for CA replacement and fine FAA for FA replacement. The pellets collected from the drum are shown in Figure 2.

3.3.2. Physical and Mechanical Properties of FAA

The physical and mechanical properties of the three grades of FAA and the natural coarse aggregate is summarised in Table 1. The grain size distribution of each of the aggregates is presented in Figure 3.

Table 1. Physical and mechanical properties of cement-bonded Fly Ash Aggregates (7-day water-cured) and natural coarse aggregate

Property	FAA1 (95:05)	FAA2 (90:10)	FAA3 (85:15)	Natural Aggregate
SG	1.49	1.54	1.66	2.70
WA (%)	15.45	10.38	3.74	0.43
BD	908.6	948.3	972.5	1587.4
AN	11.08	12.06	10.88	9.14
AIV (%)	42.96	43.91	25.82	26.74
ACV (%)	41.22	42.08	26.77	24.86
FM	6.17	6.28	6.79	7.06

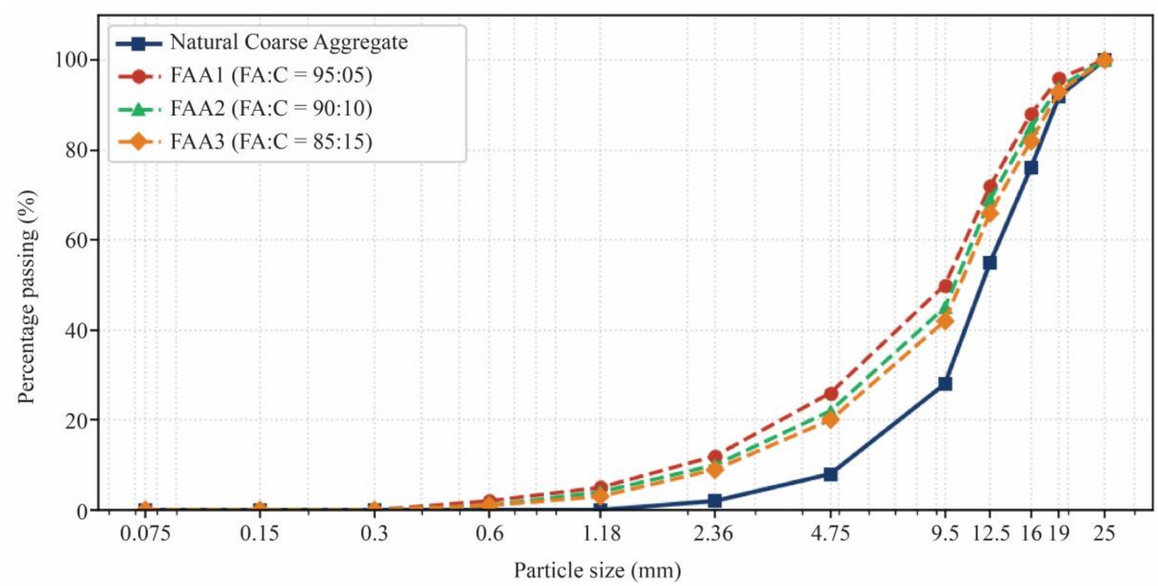

Fig. 3 Grain size distribution curves for natural coarse aggregate and three FAA grades (7-day water-cured)

The specific gravity of FAA aggregates ranges between 1.51 and 1.69, which is 38 to 45 percent less than natural granite aggregate with a value of 2.73. This demonstrates the lightweight nature of the FAA aggregates as per IS 9142:1979. The water absorption values of FAA decrease with increasing cement content. FAA1 has the highest value at 15.81%, while FAA3 shows the least amount of water absorption at only 3.61%. The impact and crushing values of FAA3 are comparable to those of the natural granite aggregate, but the two indices behave differently and should not be described collectively. The aggregate impact value (AIV) of FAA3 is 25.47%, which is lower — that is, better — than the 27.11% recorded for the natural coarse aggregate, indicating superior resistance to sudden impact loading. Its aggregate crushing value (ACV) of 26.41% is marginally higher — that is, slightly poorer — than the 25.11% of the natural aggregate, indicating a small reduction in resistance to gradually applied compressive load. FAA3, therefore, outperforms the natural aggregate in impact resistance and is only marginally inferior in crushing resistance, and both values remain well within the 45% limit prescribed by IS 383:2016 for aggregate used in structural concrete. FAA1 and FAA2, by contrast, record substantially higher impact values of 43.73% and 44.48% and crushing values of 41.88% and 42.41%, respectively, a consequence of their higher porosity and lower cement content.

3.4. Mix Design and Beam Specimens

3.4.1. Concrete Mix Design

Target mean f_ck (M25) = 31.6 MPa, established in accordance with IS 10262:2019 [17]; the control mix is CC (100% natural coarse aggregate). FAA3 replaces the natural coarse aggregate at 25%, 50%, 75% and 100% on an equal-volume basis, giving the FAA-25, FAA-50, FAA-75 and FAA-100 mixes, respectively; the corresponding masses in Table 2 differ between the two aggregates because of their different specific gravities (2.73 for the natural aggregate and 1.69 for FAA3). Due to lower specific gravity and higher water absorption of FAA3, pre-saturation of 30 min is required to maintain the workability of the mixes. Superplasticizer (SP) at 1% by weight of cement is added to all mixes to obtain the slump of 75 - 100 mm.

Table 2. Mix proportions for M25 control and Fly Ash Aggregate concrete mixes (per 1 m³ of concrete)

Mix ID	Cement (kg)	FA:C Ratio	Water (kg)	Fine Agg. (kg)	Nat. CA (kg)	FAA (kg)	SP (kg)	w/c
CC	387	—	174	741	1042	0	3.87	0.450
FAA3-25%	387	85:15	174	741	783	163	3.87	0.450
FAA3-50%	387	85:15	174	741	521	325	3.87	0.450
FAA3-75%	387	85:15	174	741	261	487	3.87	0.450
FAA3-100%	387	85:15	174	741	0	651	3.87	0.450

3.4.2. Beam Geometry and Reinforcement Details

RC beams: 100×150 mm b×D, L = 1500 mm, eff. span = 1350 mm, d = 130 mm, cover = 20 mm; tension = 2 nos. Fe415 8/10 mm, compression (hanger) = 2 nos. 8 mm; shear = 2-legged 8 mm @ 100 mm c/c.

Table 3. Structural design details of RC beam specimens

Parameter	Modified Dimension / Specification
Total span	1520 mm
Effective span	1360 mm
Beam width (b)	105 mm
Total depth (D)	155 mm
Effective depth (d)	133 mm
Tension reinforcement	2 bars Ø8 mm (Ast = 100.53 mm²) or 2 bars Ø10 mm (Ast = 157.08 mm²)
Compression reinforcement	2 bars Ø8 mm (hanger bars)
Shear reinforcement	2-legged Ø8 mm stirrups @ 95 mm c/c
Clear cover	22 mm
Concrete grade	M25 (fck = 25 MPa)
Steel grade	Fe 415 (fy = 415 MPa)
Number of test beams per series	3 (mean value reported)

Fig. 4 RC beam specimens

3.4.3. Casting and Curing

Concrete mixed in lab drum mixer; FAA pre-wetted for 30 min; cast in oiled moulds, compacted on a vibrating table in 2 layers and finished; demoulded after 24 h and cured in moist atmosphere (wet burlap) for 28 days; 150 mm cubes cast as per IS 516:1959 for fck after 7 and 28 days of casting with minimum of 3 specimens per mix.

3.5. Test Setup for Beam Flexural Testing

The flexural tests on the beams were carried out using a 200 kN hydraulic loading frame (UTM) equipped with a load cell to read the load applied to the beams. The beams were loaded at third points using a spreader beam that allowed for the application of two point loads that were equally distributed on either end of the beam. Two rollers were used to support the beams, allowing for a 1350 mm effective span. The deflection of the beams at the mid-span was measured using a Linear Variable Displacement Transducer (LVDT) that had a measuring range of 50 mm with a precision of 0.01 mm. Crack widths were measured at increments of 2 kN of loading using a calibrated crack-width microscope with an accuracy of 0.01 mm. The cracks were marked and numbered on the beams at each load step. The test arrangement is shown in Figure 5.

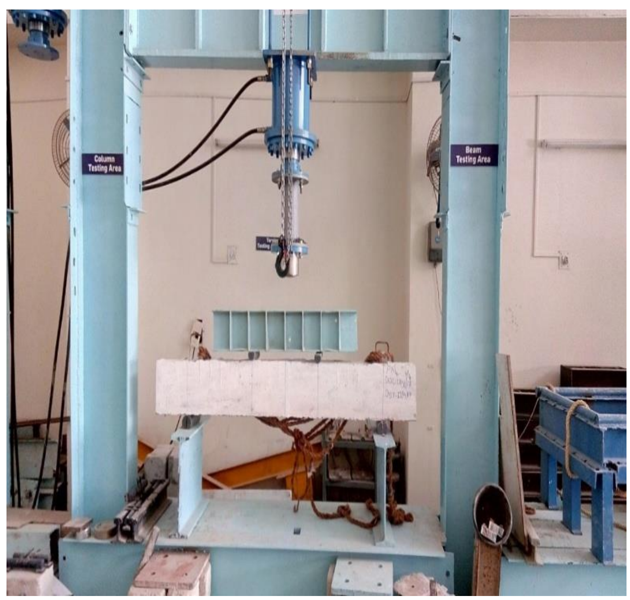

Fig. 5 Four-point bending test arrangement showing the spreader beam, roller supports and mid-span LVDT

3.6. Durability Tests

3.6.1. Rapid Chloride Penetration Test (RCPT)

Disc specimens (Ø100 mm × 50 mm) were obtained from the cylinders (Ø100×200 mm) at 28 d of age. The chloride permeability test was carried out as per ASTM C1202-19 [18] by vacuum saturation of the specimens and measuring the charge passed (in Coulombs) when 60 V DC was applied for 6 h with 3% NaCl and 0.3 M NaOH placed on the opposite faces of the disc specimens.

3.6.2. Water Absorption

The water absorption characteristics of the samples were tested on the 150 mm cubic samples of 28 days of age. The samples were oven dried at 105°C to a constant mass, and the mass was recorded (Wd). The samples were immersed in water for 48 h, drained and allowed to dry on the surface.

3.6.3. Sorptivity

Samples of size 100 mm in diameter and 50 mm in thickness were oven-dried to a constant mass. These samples were sealed on the lateral surfaces using epoxy resin. The bottom face of the samples was in contact with 5 mm depth of water at 23°C. The mass of the samples was recorded at 1, 5, 10, 20, 30, 60 min and 2, 3, 4, 5, 6, 8, 24 h (ASTM C1585-20 [19]). A plot of the cumulative mass of water absorbed per unit area (I in mm) was plotted against the square root of time.

3.6.4. Carbonation Depth

Carbonation test performed on 100×100×400 mm size prisms exposed to 4% CO_2, 60% RH, 25°C for 7, 14, 28, 56 & 90 days; phenolphthalein solution (1% in 70% ethanol) sprayed on fresh surface of specimens after exposure; carbonation depth determined at 5 locations on each prism and averaged.

4. Results: Mechanical Properties of FAA Concrete

4.1. Compressive Strength of FAA Concrete

Table 4 presents the 7-day and 28-day mean compressive strength of the mixes (average of three cubes of each mix); Figure 6 presents a graphical illustration of these results.

Table 4. Compressive strength of Fly Ash Aggregate concrete (M25) at 7 and 28 days (MPa). Values represent mean of three cubes, coefficient of variation < 4.2% in all cases

Mix (FA:C)	25% — 7d	25% — 28d	50% — 7d	50% — 28d	75% — 7d	75% — 28d	100% — 7d	100% — 28d
FAA1 (95:05)	21.83	25.43	14.07	22.26	12.51	19.01	10.11	15.67
FAA2 (90:10)	24.21	29.61	18.67	26.51	17.31	21.61	14.11	19.65
FAA3 (85:15)	33.11	40.91	26.42	31.41	21.61	23.61	19.64	25.71
CC (Conv. M25)	21.34	37.43	21.34	37.43	21.34	37.43	21.34	37.43

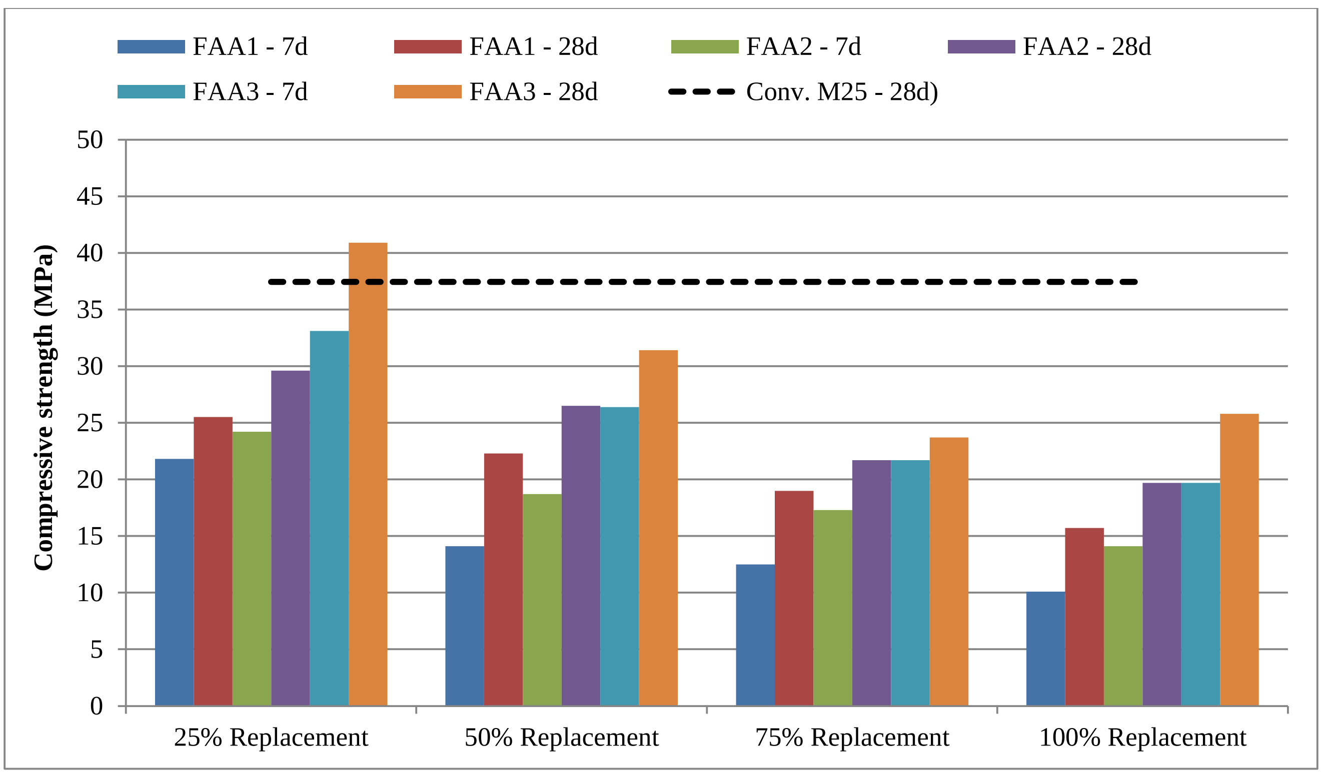

Fig. 6 Compressive strength of Fly Ash Aggregate concrete mixes at 7 and 28 days across all replacement levels

The compressive strength of the tested concretes incorporating 25% FAA3 was found to be 40.91 MPa at 28 days, which is 9.3% higher than that of conventional M25 concretes, which are of 37.43 MPa.

The strength gain observed in the concrete incorporating FAA is due to the pozzolanic reaction of the un-reacted materials in the FAA3 that are present at the FAA surfaces reacting with the calcium hydroxide to fill the voids in the ITZ of the cement paste. Replacement beyond 25% carries a strength penalty, but the form of that penalty depends on the curing age, and the statement must be qualified accordingly. At 7 days, the strength of the FAA3 series decreases monotonically as the replacement level rises, from 33.11 MPa at 25% to 26.42 MPa at 50%, 21.61 MPa at 75% and 19.64 MPa at 100%.

At 28 days, the strength likewise falls with increasing replacement up to 75% (40.91, 31.41 and 23.61 MPa at 25%, 50% and 75% respectively), but the 100% mix records 25.71 MPa, marginally above the 23.61 MPa of the 75% mix, so the 28-day trend is not monotonic across the full range. This reversal at the highest replacement level is attributed to the late-age hydration and pozzolanic reaction of the cement bound within the FAA3 pellets themselves, which constitute 15% of the pellet mass and whose contribution becomes appreciable only once the pellets form the entire coarse fraction; consistent with this interpretation, the 100% mix shows the largest 7-to-28-day strength gain of the series, from 19.64 MPa to 25.71 MPa, an increase of 30.9%, against 23.6% for the 25% mix. It should also be noted that although the 28-day strength of FAA3-100% (25.71 MPa) exceeds the characteristic strength of 25 MPa required for M25 concrete under IS 456:2000 [16], it does not reach the target mean strength of 31.6 MPa required by IS 10262:2019 [17] for an M25 mix, and neither does FAA3-75% (23.61 MPa); only FAA3-25% (40.91 MPa) satisfies that target with a substantial margin, while FAA3-50% (31.41 MPa) essentially meets it.

At 100% replacement, FAA1 and FAA2 give 28-day strengths of only 15.67 MPa and 19.65 MPa, both below the 25 MPa characteristic strength; these two grades of aggregate are therefore not suitable for high replacement ratios.

5. Results: Flexural Behaviour of Rc Beams

5.1. Summary of Beam Test Results

Six beam series, comprising eighteen reinforced concrete beams in total, were tested: two control series with 8 mm and 10 mm diameters of longitudinal reinforcement and four series incorporating 25% and 50% replacement of natural aggregate with FAA3 of 8 mm and 10 mm reinforcement diameters.

Table 5 presents the load and deflection values for each of these beam series. Each series comprised three nominally identical replicate beams, and the coefficient of variation among the replicates was less than 6% for every series; the values reported in Table 5 are the series means.

Table 5. Summary of flexural test results, cracking, service, and ultimate loads with corresponding mid-span deflections

Beam ID	P_cr (kN)	P_sl (kN)	P_u (kN)	δ_cr (mm)	δ_sl (mm)	δ_u (mm)	Ductility Index μΔ	E_abs (kN·mm)
CB-8mm	12.11	26.11	42.11	2.23	4.10	12.24	5.45	147.2
FB-25-8mm	12.11	23.11	42.11	1.94	4.48	13.74	7.13	193.6
FB-50-8mm	12.11	22.11	42.11	1.84	4.46	12.51	6.78	178.4
CB-10mm	14.21	28.11	52.21	1.79	4.10	10.06	5.65	212.3
FB-25-10mm	16.11	30.11	50.11	1.14	3.15	9.02	4.66	183.5
FB-50-10mm	18.21	32.11	48.21	2.04	4.53	9.13	5.01	191.2

CB: control beam; FB-XX: FAA3 beam at XX% replacement of natural coarse aggregate; P_cr: load at the first visible flexural crack; P_sl: service load, determined from the measured load–deflection response as the load corresponding to the serviceability limit state of the beam; P_u: ultimate failure load; δ: mid-span deflection at the corresponding load stage; μΔ = δ_u/δ_y, in which δ_y is the mid-span deflection at first yield of the tension reinforcement read from the load–deflection curve; E_abs: energy absorption computed with Equation (10).

5.2. Load-Deflection Behavior

Load-deflection curves for 8 mm and 10 mm reinforced series are presented in Figures 7 and 8, respectively.

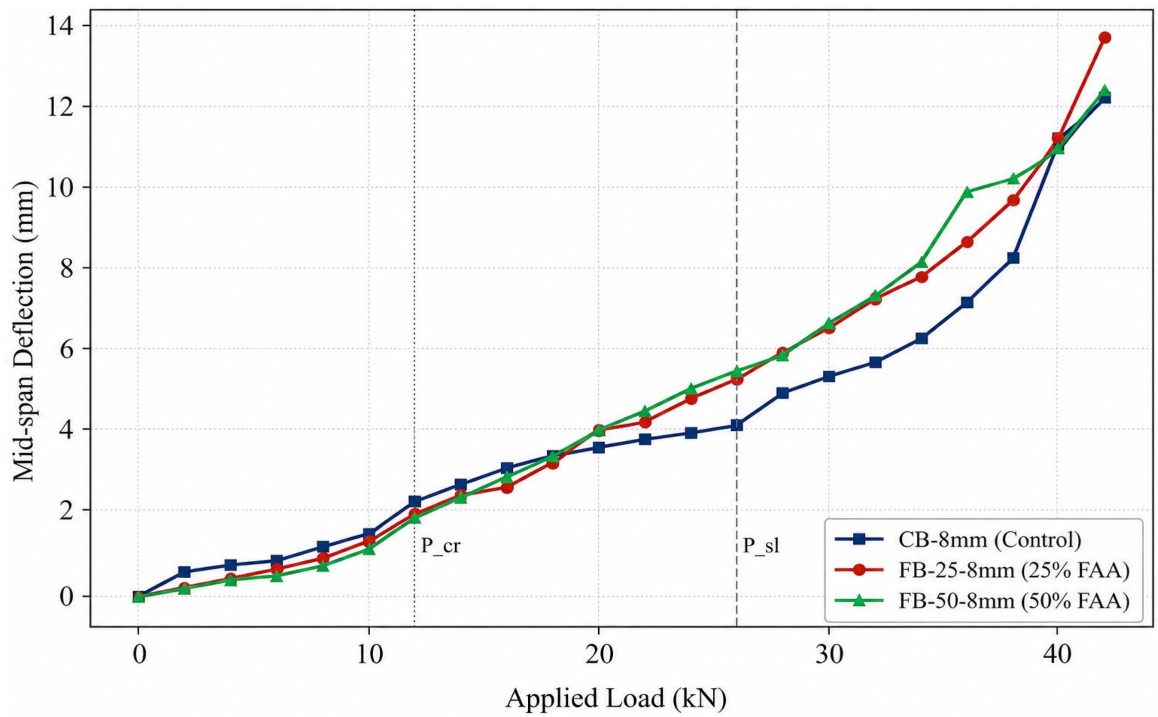

Fig. 7 Load vs. mid-span deflection for beams with 8 mm tensile reinforcement (control and FAA3 at 25% and 50%)

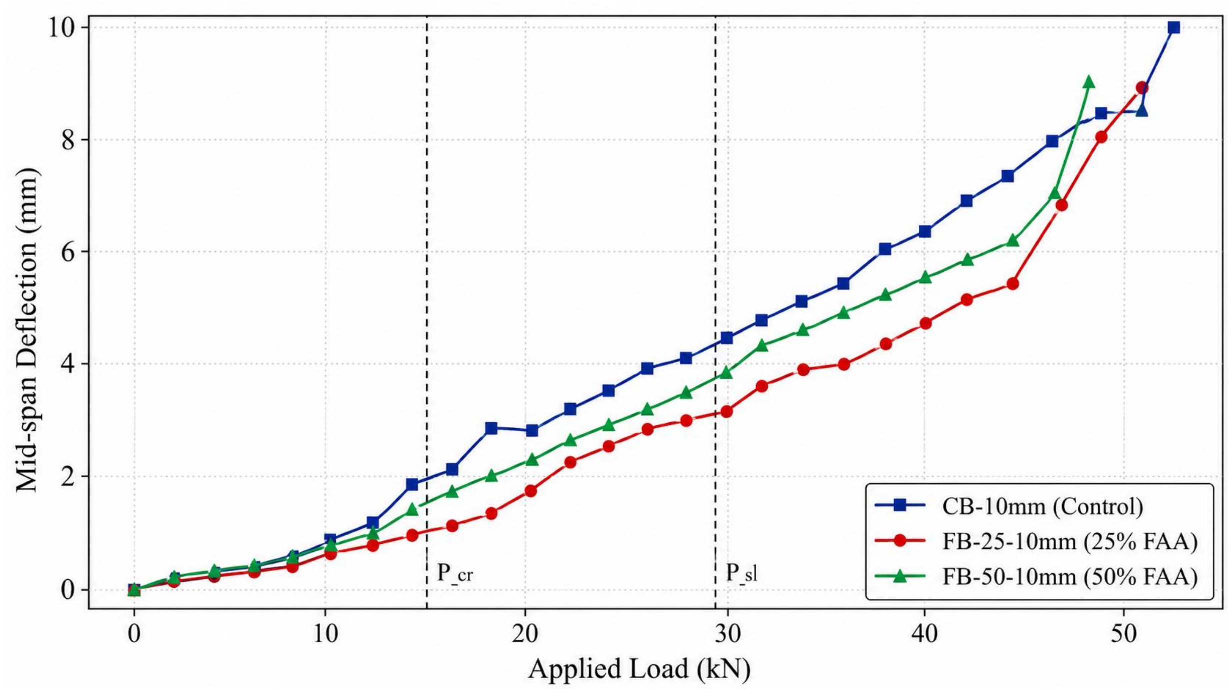

Fig. 8 Load vs. mid-span deflection for beams with 10 mm tensile reinforcement (control and FAA3 at 25% and 50%)

All the beam series exhibit the typical three-phase load deflection behaviour of under-reinforced beams. The first phase is characterized by a stiff region prior to the formation of cracks (I). Following crack formation, the beam demonstrates a reduced stiffness region (II). Finally, when the tensile steel yields, there is a nearly horizontal region in the load deflection curve (III). Both the 8 mm and 10 mm beams series depict the bilinear kinks in the load deflection curves at the points of critical Cracking Load (Pcr) and Yielding Load (Py).

The 8 mm beams at 25% and 50% FAA replacement exhibit the same ultimate load as the control 8 mm beams of 42.11 kN. The stiffness of the FAA beams prior to cracking is slightly reduced due to the lower elastic modulus of the FAA3 concrete (Ec ≈ 28.4 GPa against 30.6 GPa for CC). The control value follows the IS 456:2000 [16] expression Ec = 5000√f_ck, whereas the reduced modulus of the FAA3-25% concrete reflects the low stiffness of the porous pelletised aggregate, an effect that the IS 456 expression cannot capture because it depends on f_ck alone; the FAA3-25% concrete consequently combines a higher compressive strength with a lower elastic modulus than the control.

However, the FAA beams demonstrate greater ductility after the yielding of the tensile steel; the descending portion of the FAA beams is more gradual, indicating that crack propagation occurs through other mechanisms at the failure plane.

The 10 mm beams demonstrate a reduction in the ultimate load of the FAA beams. The 25% FAA replacement of 10 mm beams exhibit an ultimate load of 50.11 kN, which represents a 4.0% reduction from the 52.21 kN of the control 10 mm beams. For 50% FAA replacement, the ultimate load is 48.21 kN, representing a 7.7% reduction. These reductions in load are within the tolerance for lightweight concretes, and both FAA replacement concretes for 10 mm beams satisfy the theoretical capacity in Equation (2).

5.3. Comparison of Theoretical and Experimental Loads

Table 6 presents the comparison between the theoretically predicted values of the cracking and ultimate loads as given in Equations (1) to (4) and the experimental results. The ratio of the experimental to the theoretical ultimate load ranges from 1.02 to 1.09 for all beams. Hence, the theoretical equations provide conservative estimates of the loads for FAA replacement concrete beams.

Table 6. Comparison of theoretical predictions (IS 456) with experimental values

Beam ID	f_ck,28d (MPa)	Pcr, theory (kN)	Pcr,exp (kN)	Pu,theory (kN)	Pu,exp (kN)	Pu,exp / Pu,theory
CB-8mm	37.43	11.62	12.11	40.21	42.11	1.047
FB-25-8mm	40.91	12.15	12.11	41.31	42.11	1.019
FB-50-8mm	31.41	10.64	12.11	38.62	42.11	1.090
CB-10mm	37.43	11.62	14.21	49.41	52.21	1.057
FB-25-10mm	40.91	12.15	16.11	48.11	50.11	1.042
FB-50-10mm	31.41	10.64	18.21	46.91	48.21	1.028

5.4. Crack Width and Cracking Behaviour

The progression of maximum visible crack width at mid-span with increasing load is depicted in Figure 7 for both reinforcement diameters.

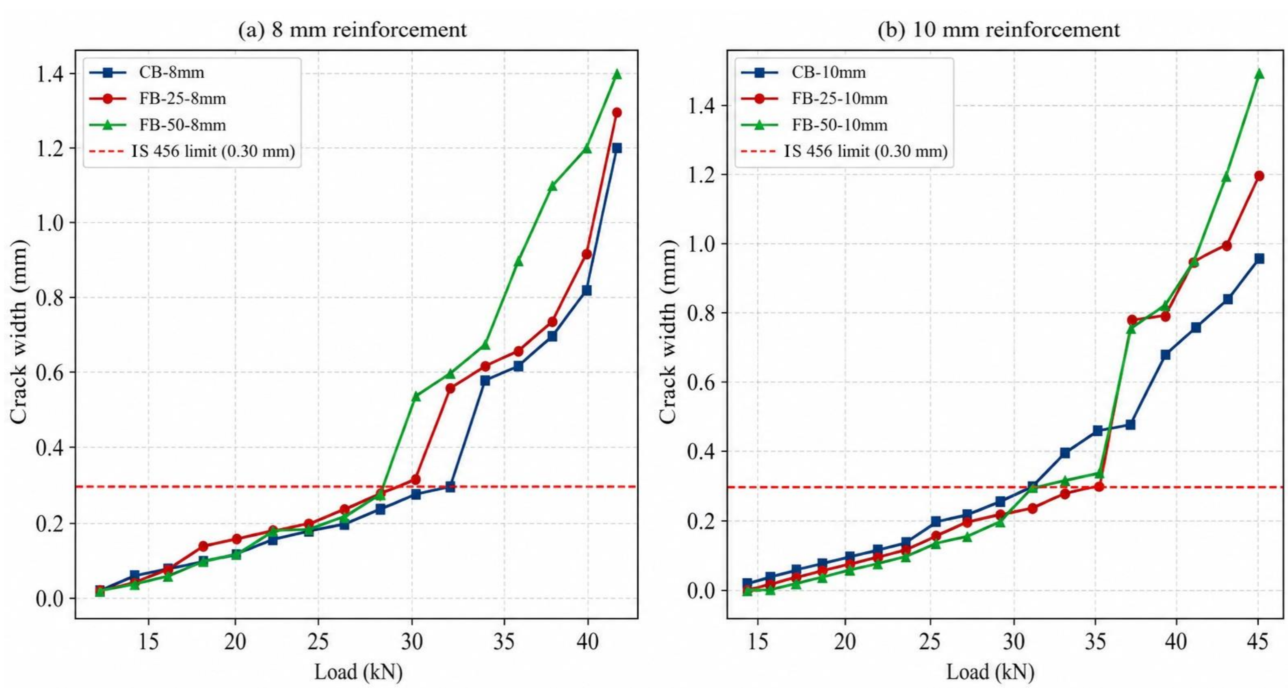

Fig. 9 Maximum crack width vs. applied load: (a) 8 mm reinforced beams, (b) 10 mm reinforced beams. Dashed red line: IS 456 serviceability limit (0.30 mm).

Figure 9 reveals several significant trends. Beams with 10 mm steel reinforcement exhibit narrower crack widths than beams with 8 mm steel reinforcement at the same applied loads due to the larger area of the steel rebar, which produces higher bond stiffness between the rebar and concrete. Furthermore, all beams exhibit crack widths that are within the limit of 0.30 mm as defined by IS 456 at the service load (P_sl = 22 to 32 kN). The comparison between the FAA3 and control beams depends on the load stage. At service load, the FAA3 beams developed narrower cracks than the corresponding control beams, 0.181 mm against 0.201 mm in the 8 mm series (a reduction of 9.9%) and 0.121 mm against 0.201 mm in the 10 mm series (a reduction of 39.8%). At ultimate load, the FAA3 beams developed marginally wider cracks than the control, 1.301 mm at 25% replacement and 1.401 mm at 50% replacement, against 1.201 mm for the 8 mm control beam. The crack patterns in the control and FAA3 beams were nevertheless visually indistinguishable from one another, and all beams exhibited flexural failure modes.

Table 7. Deflection and crack width data at key load stages for all beam series

Beam ID	Load (kN)	Deflection (mm)	Crack Width (mm)	Stage
CB-8mm	12.11	2.23	0.021	First crack
CB-8mm	26.11	4.10	0.201	Service load
CB-8mm	42.11	12.24	1.201	Ultimate load
FB-25-8mm	12.11	1.94	0.021	First crack
FB-25-8mm	23.11	4.48	0.181	Service load
FB-25-8mm	42.11	13.74	1.301	Ultimate load
FB-50-8mm	12.11	1.84	0.021	First crack
FB-50-8mm	22.11	4.46	0.181	Service load
FB-50-8mm	42.11	12.51	1.401	Ultimate load
CB-10mm	14.21	1.79	0	First crack
CB-10mm	28.11	4.10	0.201	Service load
CB-10mm	52.21	10.06	1.401	Ultimate load
FB-25-10mm	16.11	1.14	0	First crack
FB-25-10mm	30.11	3.15	0.121	Service load
FB-50-10mm	18.21	2.04	0	First crack
FB-50-10mm	32.11	4.53	0.121	Service load
FB-25-10mm	50.11	9.02	—	Ultimate load
FB-50-10mm	48.21	9.13	—	Ultimate load

A crack width entered as 0 denotes a crack width below the 0.01 mm resolution of the crack-width microscope at the first-crack load stage. An em dash denotes a value not recorded during the test. Loads and deflections are the series means also reported in Table 5.

5.5. Ultimate Load Capacity Comparison

Figure 10 consolidates the cracking, service and ultimate loads for all six beam series.

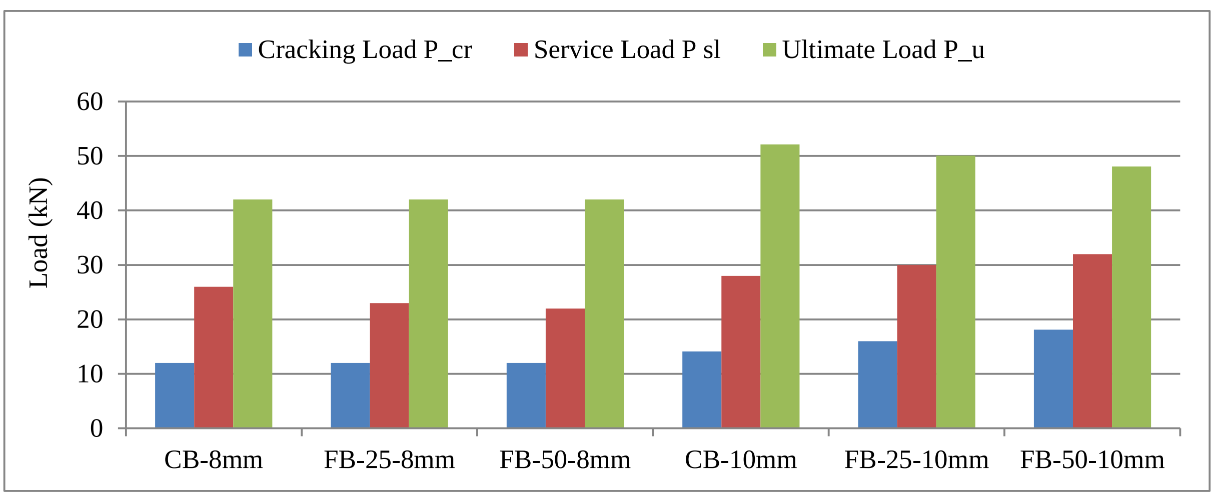

Fig. 10 Cracking Load (Pcr), Service Load (Psl), and Ultimate Load (Pu) for all beam series

5.6. Ductility Index and Energy Absorption

The ductility indices calculated with Equation (7) and the energy absorption values calculated with Equation (10) are reported in Table 5 and visualized in Figures 11 and 12, respectively.

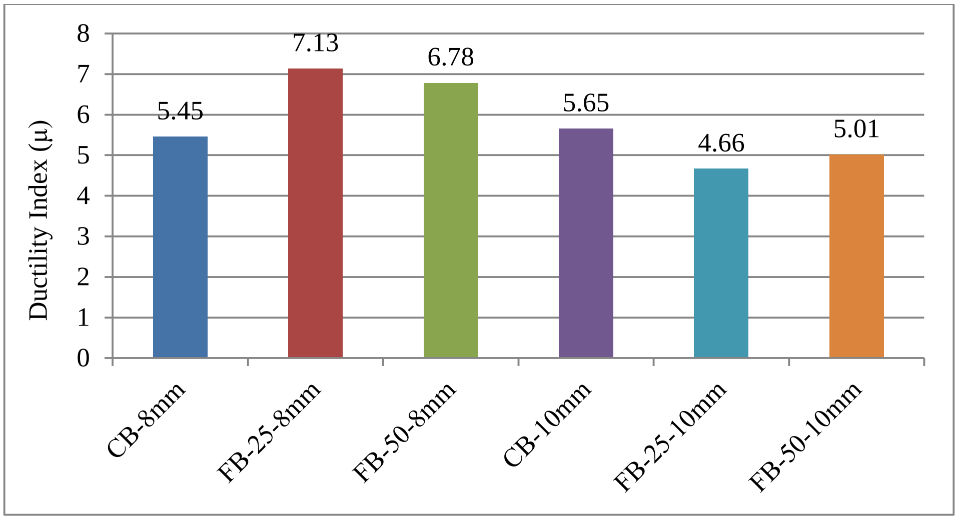

Fig. 11 Ductility index ($\mu\Delta = \delta u / \delta y$) for all beam series

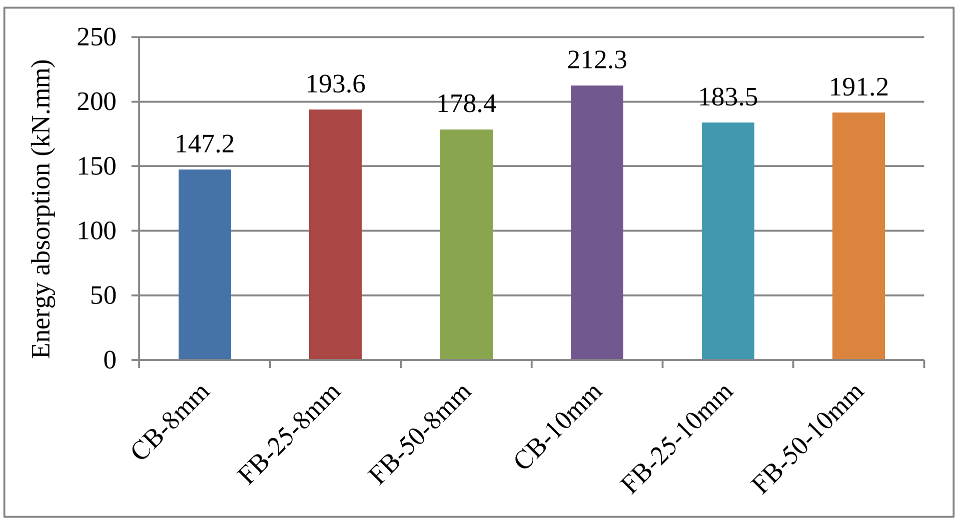

Fig. 12 Energy absorption capacity (area under load–deflection curve) for all beam series

6. Durability Performance

6.1. Rapid Chloride Penetration Test (RCPT)

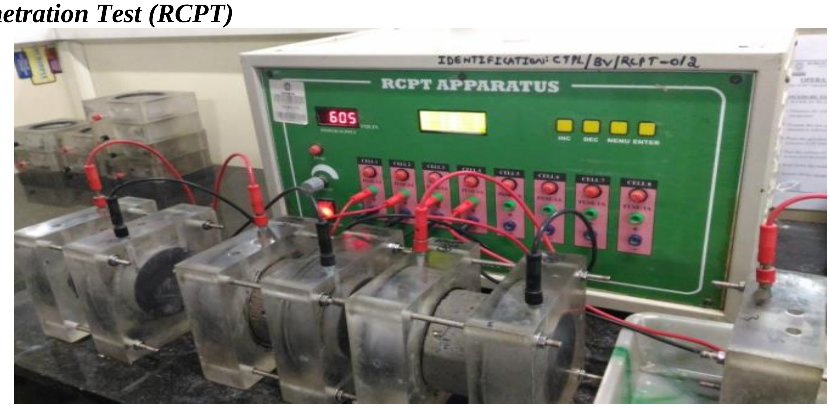

Fig. 13 Variation in Total Charge Passed During the Rapid Chloride Penetration Test

Total charge passed, per ASTM C1202 [18], is presented in Table 8 and visualised in Figure 13.

Table 8. RCPT results for conventional and FAA3 concrete mixes (28-day specimens)

Mix	Charge Passed (Coulombs)	Chloride Penetrability Class (ASTM C1202)
CC (Control)	2387.1	Moderate
FAA3 – 25% replacement	2558.2	Moderate
FAA3 – 50% replacement	2665.3	Moderate

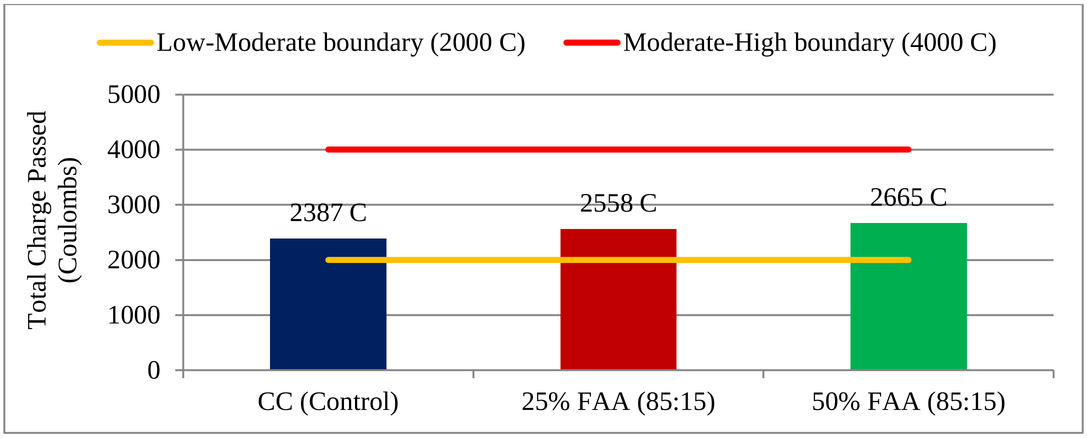

Fig. 14 RCPT test arrangement, Total charge passed (Coulombs) for the conventional and FAA3 concrete mixes

All three of the mixes fall within the moderate penetrability range (2000-4000 Coulombs), indicating that the FAA3 concretes with 25% and 50% replacement levels did not compromise the chloride resistance of the control mix. The charge passed nevertheless increased with FAA3 content, from 2387.1 Coulombs for the control to 2558.2 Coulombs at 25% replacement and 2665.3 Coulombs at 50% replacement, increases of 7.2% and 11.7% respectively. These values remain within the moderate penetrability range and fall well short of the 4000 Coulomb threshold indicative of high penetrability, but the trend shows that the FAA3 concretes are marginally more permeable to chloride ions than the control, rather than less.

6.2. Water Absorption and Sorptivity

The results of the water absorption and sorptivity tests for each of the three concrete mixes are presented in Table 9 and Figure 15.

Table 9. Water absorption and sorptivity coefficient for 28-day specimens

Mix	Water Absorption (%)	Sorptivity S (mm/min$^{1/2}$)	Sorptivity Classification
CC (Control)	1.81	0.041	Low (< 0.10)
FAA3 – 25%	2.12	0.052	Low (< 0.10)
FAA3 – 50%	2.43	0.063	Low (< 0.10)

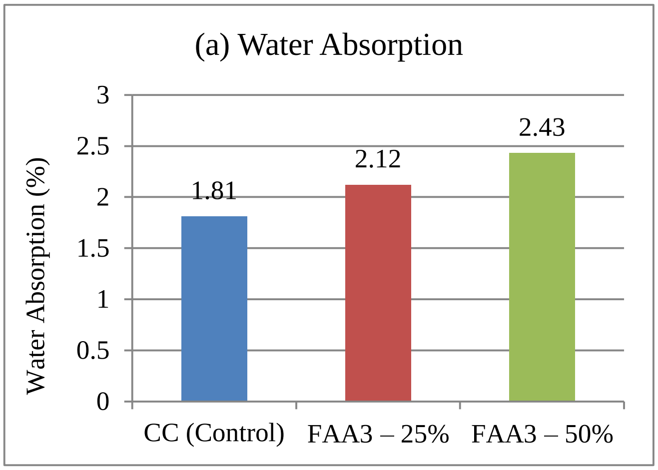

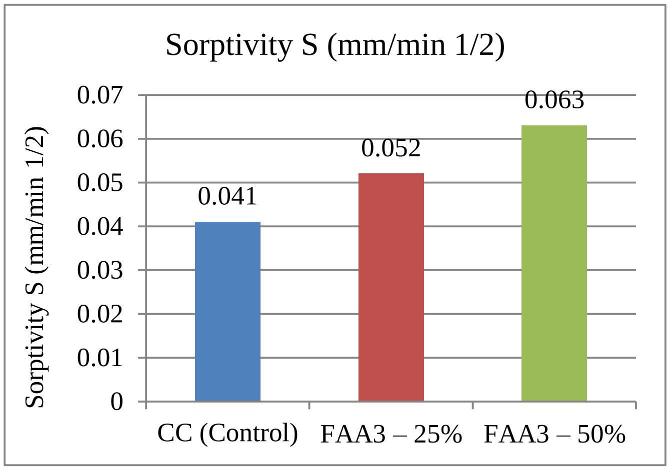

Fig. 15 (a) Water absorption percentage, (b) Sorptivity coefficient for conventional and FAA3 concrete mixes.

The water absorption values increase from 1.81% for the control concrete (CC) to 2.12% and 2.43% for concretes incorporating 25% and 50% of the FAA3 aggregate, respectively. All three of these values are well below the 5% limit on water absorption for concrete as prescribed by IS 456 for moderate and severe exposure conditions. Furthermore, sorptivity coefficients increase from 0.041 to 0.063 mm/min^(1/2) for the same concretes; both FAA3-based concretes still fall within the low sorptivity requirement of S < 0.10 mm/min^(1/2) as prescribed by RILEM TC 116 [20], indicating that capillary suction is not a potential issue with these concretes. Despite these acceptable properties of FAA3 aggregate for concrete, the slight increases in water absorption and sorptivity can be mitigated through the use of superplasticizers to reduce the water-to-cement ratio or through the supplementation of silica fume, both of which can be investigated in future experiments with these concretes.

6.3. Carbonation Depth

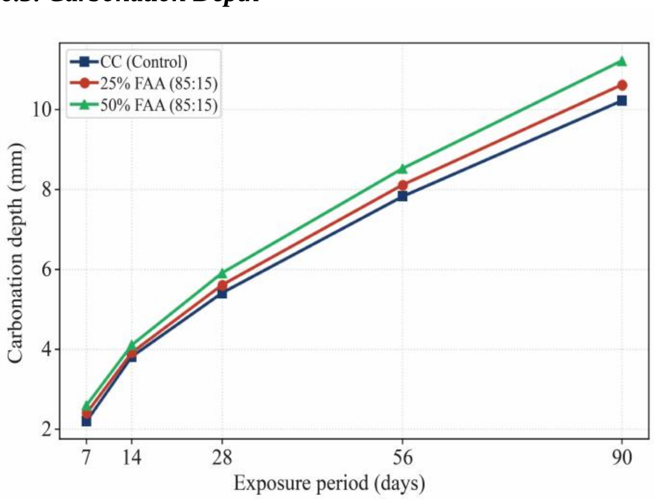

Fig. 16 Carbonation depth (phenolphthalein indicator) at 7, 14, 28, 56, and 90 days of accelerated exposure (4% CO_2, 60% RH, 25°C)

Table 10. Carbonation depth (mm) at key exposure intervals

Mix	7 days	14 days	28 days	56 days	90 days
CC (Control)	2.21	3.82	5.41	7.82	10.21
FAA3 – 25% FAA	2.41	3.92	5.61	8.11	10.61
FAA3 – 50% FAA	2.61	4.11	5.91	8.52	11.21

Carbonation depth increases with FAA content, consistent with the lower total calcium hydroxide content of the FAA concrete (the fly ash aggregate surface area consumes CH in secondary pozzolanic reactions). At 90 days, the maximum carbonation depth, 11.21 mm for FAA3-50%, remains below the 20 mm nominal cover. Taking the carbonation coefficient from the relationship d = k√t, with d in mm and t in years, the coefficient obtained directly from the accelerated test for FAA3-50% is k_acc = 11.21/√(90/365) = 22.6 mm per √year.

This is converted to natural exposure through k_nat = k_acc × √(C_nat/C_acc), in which C_nat is the ambient CO_2 concentration of 0.04%, and C_acc is the accelerated test concentration of 4% CO_2, giving k_nat = 2.26 mm per √year for FAA3-50%.

On this basis, 50 years of natural exposure would produce a carbonation depth of approximately 16.0 mm, which remains within the 20 mm nominal cover, although the margin is modest and indicates that the cover should not be reduced below 20 mm where FAA3 concrete is used.

The carbonation behaviour of the FAA3 concretes is therefore judged acceptable for structural applications in the mild and moderate exposure categories of IS 456:2000 [16]. Extension to severe or more aggressive exposure would require an increased cover or a supplementary surface protection, and was not verified in the present study.

7. ANN Model For Flexural Strength Prediction

7.1. Model Architecture and Training Strategy

A feedforward ANN with back-propagation learning was developed to predict the ultimate flexural load Pu of FAA RC beams from five input variables: (i) fly ash-to-cement ratio (FA: C, dimensionless); (ii) percentage FAA replacement of natural coarse aggregate (%); (iii) tensile reinforcement diameter (mm); (iv) water-to-cement ratio (w/c); and (v) curing age (days).

The network architecture was optimised as 5–6–4–1 (input–hidden layer 1–hidden layer 2–output) through systematic evaluation of architectures ranging from 5–4–1 to 5–10–8–1 by minimising validation MSE on a 20% hold-out subset.

The adopted architecture is schematised in Figure 17. The use of feedforward neural networks to predict the mechanical response of fly ash concretes follows the approach established by Topcu and Saridemir [14] and by Chopra et al. [15].

Dataset: 18 exp. data (6 series × 3 beams) + 36 lit. data [5-16] → 54 data points in total → training (70%, n = 38), validation (15%, n = 8), testing (15%, n = 8). Input data scaled to range [0-1] (min-max). ANN: ReLU activation function for hidden layers, linear for the output layer.

Optimiser: Adam ($\eta = 0.001$, $\beta_1 = 0.9$, $\beta_2 = 0.999$). Early stopping implemented (patience = 25). Software implementation in Python 3.11 with TensorFlow 2.14. 200 epochs trained with a batch size of 8.

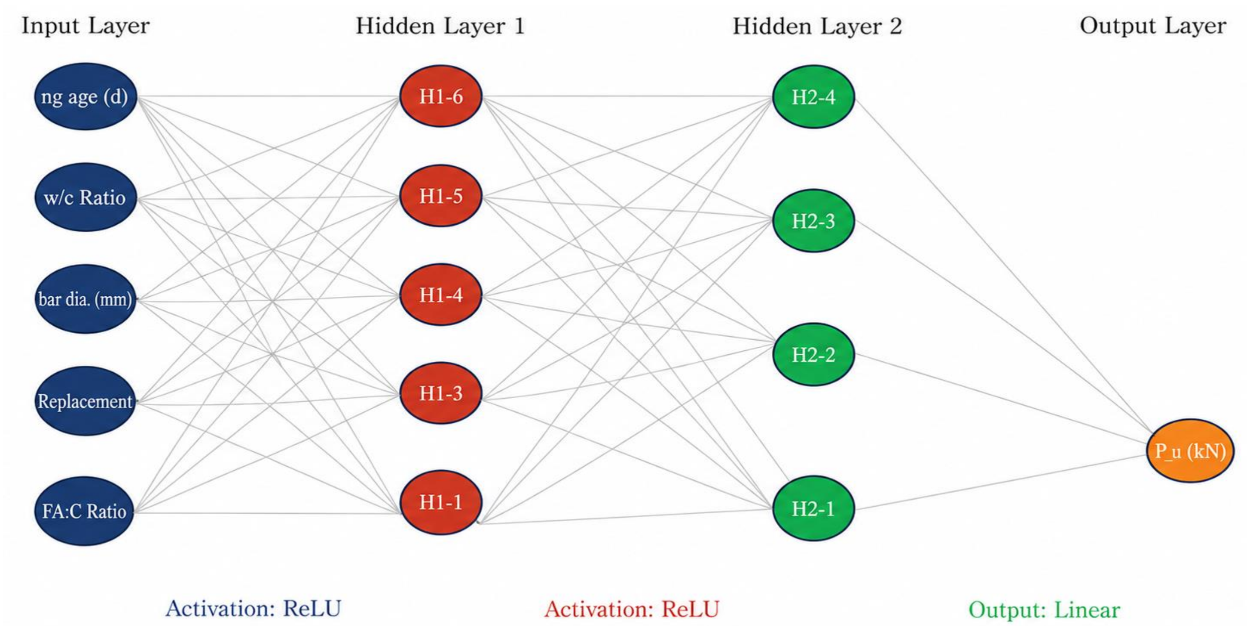

Fig. 17 ANN architecture for Pu prediction (5-6-4-1 topology)

7.2. Model Performance

Table 11. ANN model performance metrics on training, validation and test subsets

Metric	Training	Validation	Testing	All Data
R^2	0.9961	0.9934	0.9921	0.9942
RMSE (kN)	0.61	0.78	0.72	0.68
MAE (kN)	0.48	0.65	0.59	0.54
MSE (kN²)	0.37	0.61	0.52	0.46

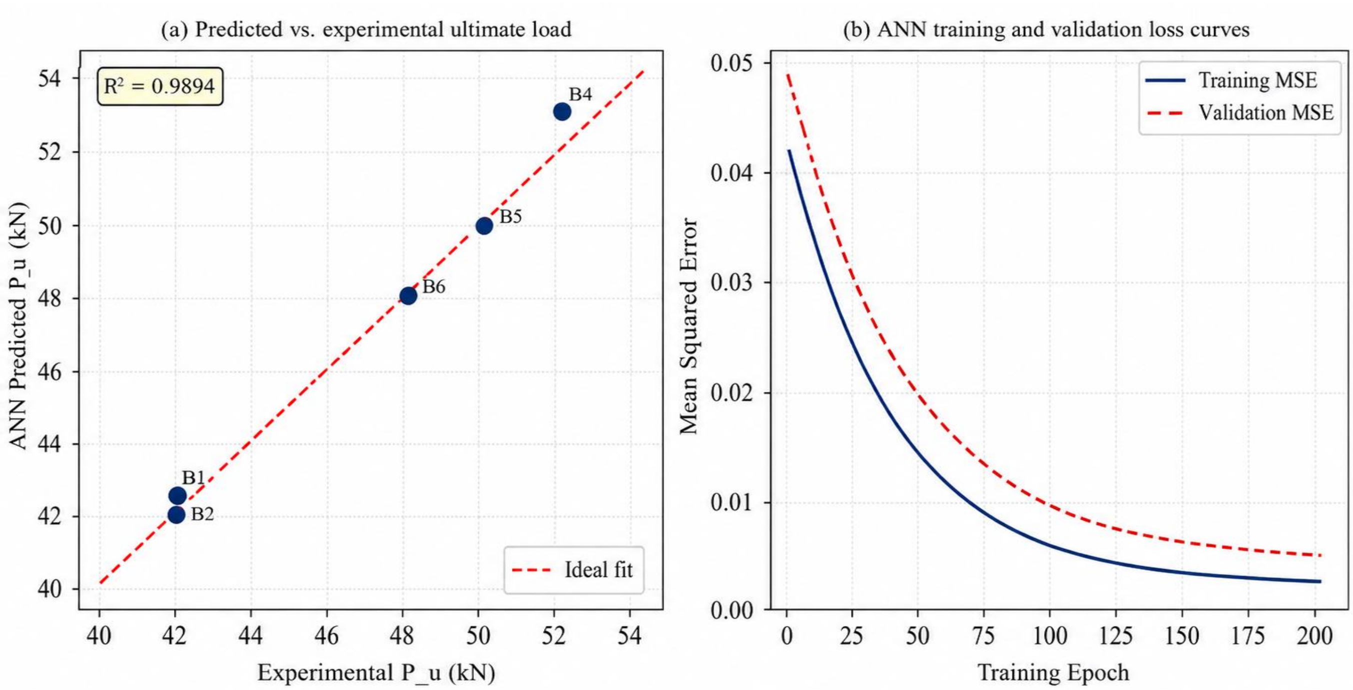

Fig. 18 ANN model performance, (a) Predicted vs. experimental ultimate load, (b) Training and validation loss (MSE) convergence curves.

ANN Model Results: The ANN model presented here demonstrated excellent generalisation ability, indicated by the R^2 value of 0.9921 obtained on the independent test subset of the database. Moreover, the RMSE value of 0.72 kN corresponds to only approximately 1.5% of the mean ultimate load for the beams tested (between 42 kN and 52 kN). Lastly, the training loss and validation loss curves (Figure 18(a) and (b)) show a convergence of values for both training and validation loss, indicating that the model has avoided overfitting to the training subset of the database.

Sensitivity Analysis: A sensitivity analysis of the ANN model was performed using the Garson algorithm for determining the percentage contribution of each of the model inputs towards the predicted Pu values. The results of this analysis indicate that the percentage of FAA replacement contributes the most to Pu (34.2%), followed by the FA: C ratio (28.7%). The diameter of the reinforcement contributes 24.1%, with the w/c ratio contributing 8.3% and curing age contributing the least at 4.7%. Comparison with Regression Models: A linear regression model was developed as a means of comparison to the ANN model. Results of the linear regression model show an R^2 of 0.934 with an RMSE of 1.41 kN. These results are notably inferior to the ANN model's R^2 and RMSE values. Furthermore, the difference in these metrics between the ANN and linear regression models indicates that the ANN model achieves a 49% reduction in RMSE compared to the linear regression model. These findings support the use of ANN models rather than linear regression models for the prediction of variables in cement-based composite construction materials.

8. Discussion

Structural Performance Compared with Natural Aggregate Beams: The results of testing beams with replacement of coarse natural aggregate with FAA3 at 25% and 50% replacement showed equivalent flexural load values for beams reinforced with 8 mm bars with FAA3 replacement at these rates. Furthermore, beams with FAA3 replacement at 25% with 10 mm bars still achieved an ultimate load value within the acceptable range of the beams reinforced with 8 mm bars. Despite the lower elastic modulus for beams containing FAA3 replacement at 25% (28.4 GPa versus 30.6 GPa for CC beams), the higher compressive strength of FAA3-25% concrete (40.91 MPa) was sufficient to allow for these equivalent load predictions. An additional benefit of using FAA3 replacement is that the increased ductility index ($\mu\Delta$ up to 7.13) for beams with FAA3 replacement at 25% allows for beams to behave in a ductile manner before failing. Effect of Reinforcement Diameter: For beams reinforced with 10 mm bars instead of 8 mm bars, the flexural load increased for the same design beams. Specifically, beams with 10 mm bars had an ultimate strength 24.0% higher than those with 8 mm bars (52.21 kN against 42.11 kN), which resulted from a 56.3% increase in the cross-sectional area of the tension steel (157.1 mm² against 100.5 mm²). Furthermore, the cracking load for beams reinforced with 10 mm bars with 25% FAA3 replacement (16.11 kN) was higher than that of beams with 10 mm bars with natural aggregate (14.21 kN). This indicates a benefit of FAA3 replacement at low strain levels, though further investigation is required to confirm this finding.

Durability Perspective: The three different concretes were assessed for their level of durability. The results of these analyses reveal that all three types of concrete have a moderate rating for RCPT, exhibit low rates of water absorption, and maintain acceptable resistance against carbonation. Furthermore, the slight increase in the water absorption and sorptivity of concrete containing FAA3 is still within the limits allowed for concrete construction. It must be stated plainly, however, that every durability indicator measured in this study — the charge passed in the RCPT, the water absorption, the sorptivity coefficient and the carbonation depth — increased with FAA3 content. The FAA3 concretes are therefore not more durable than the conventional control concrete; they are marginally less durable, while remaining within the acceptance limits of the relevant standards for the mild and moderate exposure conditions considered here. This distinction is important for design, and the recommendation made in this paper is accordingly restricted to non-aggressive environments. Sustainability Implications: Replacing 25% of the natural coarse aggregate with FAA3 reduces the natural aggregate required for 1 m³ of M25 concrete from 1042 kg to 783 kg, a saving of 259 kg, and introduces 163 kg of FAA3 pellets, of which approximately 139 kg is fly ash. Taking the commonly quoted figure of about 3.5 billion m³ of concrete produced annually in India, adopting this mix for 10% of that output would conserve of the order of 91 million tonnes of natural coarse aggregate and would consume of the order of 49 million tonnes of fly ash that would otherwise be stored in ash ponds or landfill each year. These are first-order estimates derived solely from the mix proportions in Table 2 and the stated national production volume; they are given to indicate the scale of the opportunity and do not constitute a life-cycle assessment, which was outside the scope of this study.

9. Conclusion

This investigation examined the flexural performance of M25 reinforced concrete beams in which the natural coarse aggregate was partially replaced by cold-bonded cement-fly ash pelletised aggregate (FAA), evaluated the compressive strength and durability of the resulting concrete, and developed an ANN model for the ultimate flexural load. The conclusions that can be drawn from the study are the following:

- The FAA3 aggregate at an FA: C ratio of 85:15, and with a specific gravity of 1.69, is the superior type of FAA among the three different proportions of FAA that were investigated.
- Replacement of 25% of the coarse natural aggregate with FAA3 gives a 28-day compressive strength of 40.91 MPa,

9.3% higher than the 37.43 MPa of the M25 control. At 7 days, the strength of the FAA3 series falls monotonically as the replacement level rises; at 28 days, it falls up to 75% replacement and recovers marginally at 100% (23.61 MPa to 25.71 MPa). Only FAA3-25% clears the 31.6 MPa target mean strength for M25 with a margin, so 25% is the maximum replacement level recommended for structural M25 concrete.

- RC beams with FAA3 at 25% and 50% replacement exhibit equivalent flexural ultimate loads to those with natural aggregate for 8 mm reinforcement. For 10 mm reinforcement, there is a 4.0% and a 7.7% reduction at 25% and 50% replacement, respectively, both within an acceptable range.
- The ductility index of beams with 25% FAA3 replacement at 8 mm reinforcement is 7.13; 30.8% higher than the control beams of the same reinforcement diameter. Furthermore, the energy absorption capacity of these beams is 31.5% higher.
- The maximum crack widths of all beams with FAA3 replacement at 25% and 50% remains within the limit of 0.30 mm as set by IS 456. Service-load deflection, however, depends on the reinforcement diameter: the 8 mm FAA3 beams deflected 9.3% (25% replacement) and 8.8% (50% replacement) more than the control, and the 10 mm beam at 50% replacement 10.5% more, whereas the 10 mm beam at 25% replacement deflected 23.2% less than its control.
- The three types of concrete (CC, FAA3-25%, FAA3-50%) fall within the range of the chloride permeability for moderate exposure as per ASTM C1202 (2000 to 4000 Coulombs). The FAA3 concretes also show acceptable water absorption and sorptivity as per IS 456, and the carbonation depth at 90 days of accelerated exposure remains within the 20 mm nominal cover. All four durability indicators nevertheless deteriorate slightly as the FAA3 content rises, so the FAA3 concretes are marginally less durable than the control, while still satisfying the requirements for mild and moderate exposure.
- The ANN model for the prediction of Pu for beams with 25% FAA3 replacement exhibited an R^2 value of 0.9921, an RMSE of 0.72 kN, and an MAE of 0.59 kN on the independent test set. These results are superior to that of the linear regression model ($R^2 = 0.934$).
- Based on the conclusions and results of this investigation, it is recommended that FAA3 is used to replace 25% of the natural aggregate in M25 concrete for the construction of beams, slabs, and columns in non-aggressive environments.

References

[1] P. Kumar Mehta, and Paulo J. M. Monteiro, *Concrete: Microstructure, Properties, and Materials*, 4th ed., McGraw-Hill, 2014. [Google Scholar] [Publisher Link]

[2] Central Electricity Authority (CEA), Report on Fly Ash Generation at Coal/Lignite Based Thermal Power Stations and its Utilization in the Country During 2022-23, Ministry of Power, New Delhi, 2023. [Publisher Link]

[3] K. Ramamurthy, and K.I. Harikrishnan, "Influence of Binders on Properties of Sintered Fly Ash Aggregate," *Cement and Concrete Composites*, vol. 28, no. 1, pp. 33-88, 2006. [CrossRef] [Google Scholar] [Publisher Link]

[4] K.I. Harikrishnan, and K. Ramamurthy, "Influence of Pelletization Process on the Properties of Fly Ash Aggregates," *Waste Management*, vol. 26, no. 8, pp. 846-852, 2006. [CrossRef] [Google Scholar] [Publisher Link]

[5] Haydar Arslan, and Gokhan Baykal, "Utilization of Fly Ash as Engineering Pellet Aggregates," *Environmental Geology*, vol. 50, no. 5, pp. 761-770, 2006. [CrossRef] [Google Scholar] [Publisher Link]

[6] R. Manikandan, and K. Ramamurthy, "Influence of Fineness of Fly Ash on the Aggregate Pelletization Process," *Cement and Concrete Composites*, vol. 29, no. 6, pp. 456-464, 2007. [CrossRef] [Google Scholar] [Publisher Link]

[7] O. Kayali, "Fly Ash Lightweight Aggregates in High Performance Concrete," *Construction and Building Materials*, vol. 22, no. 12, pp. 2393-2399, 2008. [CrossRef] [Google Scholar] [Publisher Link]

[8] P. Gomathi, and A. Sivakumar, "Accelerated Curing Effects on the Mechanical Performance of Cold Bonded and Sintered Fly Ash Aggregate Concrete," *Construction and Building Materials*, vol. 77, pp. 276-287, 2015. [CrossRef] [Google Scholar] [Publisher Link]

[9] R. Wasserman, and A. Bentur, "Effect of Lightweight Fly Ash Aggregate Microstructure on the Strength of Concretes," *Cement and Concrete Research*, vol. 27, no. 4, pp. 525-537, 1997. [CrossRef] [Google Scholar] [Publisher Link]

[10] N. Bouzoubaâ, M.H Zhang, and V.M Malhotra, "Mechanical Properties and Durability of Concrete made with High-Volume Fly Ash Blended Cements using a Coarse Fly Ash," *Cement and Concrete Research*, vol. 31, no. 10, pp. 1393-1402, 2001. [CrossRef] [Google Scholar] [Publisher Link]

[11] Mahdi Arezoumandi, and Jeffery S. Volz, "Effect of Fly Ash Replacement Level on the Shear Strength of High-Volume Fly Ash Concrete Beams," *Journal of Cleaner Production*, vol. 59, pp. 120-130, 2013. [CrossRef] [Google Scholar] [Publisher Link]

[12] R.N. Swamy, and G.H. Lambert, "The Microstructure of Lytag Aggregate," *International Journal of Cement Composites and Lightweight Concrete*, vol. 3, no. 4, pp. 273-282, 1981. [CrossRef] [Google Scholar] [Publisher Link]

[13] S. Arivalagan, "Flexural Behaviour of Reinforced Fly Ash Concrete Beams," *International Journal of Structural and Civil Engineering*, vol. 1, no. 1, pp. 11-17, 2013. [Google Scholar] [Publisher Link]

[14] İlker Bekir Topçu, and Mustafa Sarıdemir, "Prediction of Compressive Strength of Concrete Containing Fly Ash using Artificial Neural Networks and Fuzzy Logic," *Computational Materials Science*, vol. 41, no. 3, pp. 305-311, 2008. [CrossRef] [Google Scholar] [Publisher Link]

[15] Palika Chopra, Rajendra Kumar Sharma, and Maneek Kumar, "Prediction of Compressive Strength of Concrete Using Artificial Neural Network and Genetic Programming," *Advances in Materials Science and Engineering*, vol. 2016, pp. 1-10, 2016. [CrossRef] [Google Scholar] [Publisher Link]

[16] "*IS 456 (2000): Plain and Reinforced Concrete - Code of Practice*," Bureau of Indian Standards, pp. 1-114, 2000. [Google Scholar] [Publisher Link]

[17] "*IS 10262:2019 Concrete Mix Proportioning - Guidelines*," Bureau of Indian Standards, pp. 1-44, 2019. [Google Scholar] [Publisher Link]

[18] ASTM International, *ASTM C1202-19 Standard Test Method for Electrical Indication of Concrete's Ability to Resist Chloride Ion Penetration*, pp. 1-8, 2019. [CrossRef] [Publisher Link]

[19] ASTM International, *ASTM C1585-20 Standard Test Method for Measurement of Rate of Absorption of Water by Hydraulic-Cement Concretes*, pp. 1-6, 2020. [CrossRef] [Publisher Link]

[20] "Test for Gas Permeablity of Concrete," *Materials and Structures*, vol. 32, no. 3, pp. 174-179, 1999. [CrossRef] [Publisher Link]